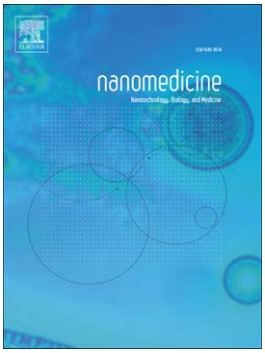

Cytoskeletal re-arrangement in TGF-β1-induced alveolar epithelial-mesenchymal transition studied by atomic force microscopy and high-content analysis

Stephen T. Buckley, Carlos Medina, Anthony M. Davies, Carsten Ehrhardt

PII: S1549-9634(11)00274-7
DOI: doi:10.1016/j.nano.2011.06.021
Reference: NANO 502

To appear in: *Nanomedicine: Nanotechnology, Biology and Medicine*

Received date: 7 December 2010
Revised date: 23 June 2011
Accepted date: 28 June 2011

Please cite this article as: Buckley Stephen T., Medina Carlos, Davies Anthony M., Ehrhardt Carsten, Cytoskeletal re-arrangement in TGF-β1-induced alveolar epithelial-mesenchymal transition studied by atomic force microscopy and high-content analysis, *Nanomedicine: Nanotechnology, Biology and Medicine* (2011), doi:10.1016/j.nano.2011.06.021

Cytoskeletal re-arrangement in TGF-β1-induced alveolar epithelial-mesenchymal transition studied by atomic force microscopy and high-content analysis

Stephen T. Buckley, PhD[1], Carlos Medina, MD, PhD[1], Anthony M. Davies, PhD[2], Carsten Ehrhardt, PhD[1]

[1]School of Pharmacy and Pharmaceutical Sciences, Trinity College Dublin, Dublin 2, Ireland

[2]Department of Clinical Medicine, Trinity College Dublin, Dublin 8, Ireland

Short title: Cytoskeletal changes in alveolar EMT by AFM and HCA

Correspondence should be addressed to:
Dr. Carsten Ehrhardt, School of Pharmacy and Pharmaceutical Sciences, Trinity College Dublin, Panoz Institute, Dublin 2, Ireland, tel.: +353-1-896-2441, fax: +353-1-896-2783, e-mail: ehrhardc@tcd.ie

Sources of support for research: S.T.B. is funded by an IRCSET Government of Ireland Postgraduate Scholarship in Science, Engineering and Technology. C.M. is SFI Stokes lecturer. This work has been funded in part by a Strategic Research Cluster grant (07/SRC/B1154) under the National Development Plan co-funded by EU Structural Funds and Science Foundation Ireland. This work was also partially supported by Science Foundation Ireland (grant no. 07/IN1/B931)

Complete manuscript word count: 6014

Number of figures: Six

Number of tables: Two

Abstract

Epithelial-mesenchymal transition (EMT) is closely implicated in the pathogenesis of idiopathic pulmonary fibrosis. Associated with this phenotypic transition is acquisition of an elongated cell morphology and establishment of stress fibres. The extent to which these EMT-associated changes influence cellular mechanics is unclear. We assessed the bio-mechanical properties of alveolar epithelial cells (A549) following exposure to TGF-β1. Using atomic force microscopy, changes in cell stiffness and surface membrane features were determined. Stimulation with TGF-β1 gave rise to a significant increase in stiffness, which was augmented by a collagen I matrix. Additionally, TGF-β1-treated cells exhibited a rougher surface profile with notable protrusions. Simultaneous quantitative examination of the morphological attributes of stimulated cells using an image-based high-content analysis system revealed dramatic alterations in cell shape, F-actin content and distribution. Together, these investigations point to a strong correlation between the cytoskeletal-associated cellular architecture and the mechanical dynamics of alveolar epithelial cells undergoing EMT.

Keywords

Actin fibres; Idiopathic pulmonary fibrosis; extracellular matrix; scanning probe microscopy; A549 cell line

List of abbreviations

AFM	atomic force microscopy
ATCC	American Type Culture Collection,
DMEM	Dulbecco's modified Eagle's medium
ECACC	European Collection of Animal Cell Cultures
ECM	extracellular matrix
EMT	epithelial-mesenchymal transition
FBS	foetal bovine serum
HCA	high-content analysis
IPF	idiopathic pulmonary fibrosis
PBS	phosphate-buffered saline
R_q	root mean square roughness
R_t	peak-to-valley roughness
TGF-β1	transforming growth factor-beta 1
TRITC	tetramethyl rhodamine isothiocyanate

1. Introduction

Idiopathic pulmonary fibrosis (IPF) is a chronic pulmonary disease of largely unknown aetiology, characterised by progressive fibrotic changes which ultimately lead to irreversible distortion of the lung architecture [1]. Central to this pathogenesis is the formation of fibrotic foci, consisting predominantly of activated myofibroblasts [2]. Whilst the precise origin of these fibrogenic myofibroblasts has yet to be fully elucidated, cumulative evidence suggests that epithelial-mesenchymal transition (EMT) of resident cells of the alveolar epithelium, a process whereby these cells lose their characteristic structural and biochemical attributes and adopt features typical of a mesenchymal phenotype, may be one such possible source [3,4]. Moreover, in support of this, a collection of cytokines are known to be activated in IPF, and a number of these have been shown to promote EMT (e.g., TGF- β1).

Implicit in this conversion from epithelial to mesenchymal phenotype are distinct alterations in cellular morphology, architecture, adhesion and migratory capacity [5]. In particular, a hallmark of EMT and loss of epithelial function is the formation of actin stress fibres [6]. This results in dynamic changes in the structure of the cytoskeleton, endowing affected cells with a spindle-shaped morphology. Notably, the impact of these structural modifications on cell mechanical properties remains poorly understood. The stiffness of the cytoskeleton is determined to a great extent by the actin network [7]. Thus, conceivably, given the dramatic acquisition of actin stress fibres during alveolar EMT, such changes should also be reflected in alterations in the mechano-elastic properties of the cells. In particular, EMT may represent a potential contributor to the abnormal tissue hardening observed in IPF. In this regard,

measuring the viscoelastic properties of transitioning living cells should provide novel insights into the influence of EMT-associated cytoskeletal restructuring on the stiffening of lung parenchyma and reveal to what extent the elastic properties are caused by cellular components, particularly parts of the cytoskeleton.

The extracellular matrix (ECM) provides a dynamic support structure on which epithelial cells can grow. Moreover, it also serves to influence cellular behaviour (e.g., migration, proliferation and morphology) [8]. Indeed, evidence indicates that ECM possesses the capacity to bring about transformation of epithelium to mesenchyme [9]. Although the primary inducer of EMT is TGF-β1, the importance of the ECM is becoming increasingly apparent, with recent studies suggesting that these components influence and augment the pro-fibrotic effects of TGF-β1 [10-13]. Additionally, from a bio-mechanical perspective, it is known that through its interactions with alveolar epithelial cells, the ECM exerts important centrifugal tethering forces, which serve to balance those centripetal forces exerted by the cytoskeleton [14]. Specifically, a number of studies in different cell types have shown that collagen I, a major component of the basement membrane in fibrotic tissues, may serve to induce EMT [10,12].

In this study, we used atomic force microscopy (AFM) to examine the mechanical stiffness of cells in response to TGF-β1, and the influence of the ECM component, collagen I, on this process. Moreover, using high-content analysis (HCA) immunofluorescence imaging techniques, we were able to comprehensively quantify the morphological changes induced by TGF-β1 stimulation, and correlate it with those observations made using AFM imaging and force measurement analysis. Together,

this enabled us to reveal the crucial importance of the actin network in determination of the structural and mechanical properties of alveolar epithelial cells during EMT. To our knowledge, this is the first such study which utilises both AFM and HCA as novel tools to assess EMT *in vitro*.

2. Methods

2.1. Materials

Hoechst 33258 was purchased from Invitrogen (Karlsruhe, Germany). Recombinant human TGF-β1 was purchased from PeproTech (London, UK). Cell culture medium, foetal bovine serum, TRITC-phalloidin and all other reagents were purchased from Sigma-Aldrich (Dublin, Ireland).

2.2. Cell culture conditions

A549 human alveolar epithelial cells (American Type Culture Collection, ATCC CL-185) were obtained from the European Collection of Animal Cell Cultures (ECACC, Salisbury, UK) and used between passage numbers 65 and 80. Cells were maintained in a 1:1 mixture of Dulbecco's modified Eagle's medium and Ham's nutrient mixture F-12 medium (DMEM/F-12) supplemented with 5% (v/v) FBS, 100 U/ml penicillin and 100 μg/ml streptomycin. Cells were cultured at 37°C in 5% CO_2 atmosphere and culture media was exchanged every 48 h. For live cell AFM studies, A549 monolayers were cultured in 6-well plates containing 24 mm glass cover slips. In AFM studies using fixed cells, A549 monolayers were grown in chamber slides (Nunc, Roskilde, Denmark). For HCA analysis, cells were cultured in 96-well plates (Nunc). Where cells were cultured on a collagen I substrate, a solution of rat tail collagen I was diluted using sterile water and each well was coated at a concentration of 20 μg/ml. The protein was allowed to bind for several hours at room temperature after which the excess fluid was removed and each well washed twice with PBS. In all studies, following one day in culture, cell medium was replaced with that containing 1% FBS and cells were treated with TGF-β1 (5 ng/ml) for 48 h.

2.3 High-content analysis (HCA)

Following culturing as detailed above, A549 monolayers were subsequently fixed by gently adding an equal volume of pre-warmed (37°C) 8% paraformaldehyde to culture medium for 15 min at 37°C. The cells were then permeabilised with 0.1% Triton X-100 in PBS for 5 min, before being washed three times with 1% bovine serum albumin (BSA)/PBS. The cells were then incubated with TRITC-phalloidin to visualise filamentous (F-)actin and Hoechst 33258 to counter-stain the cell nuclei, for 30 min at 37°C. Following three washes using 1% (w/v) BSA/PBS, the plates were resuspended in PBS and stored at 4°C in the dark until further analysis. The 96-well plates were imaged using an InCell 1000™ Analyser Cellular Imaging and Analysis platform (GE Healthcare, Piscataway, NJ). A total of 15 fields per well were imaged under 20x magnification using 2 separate filters to capture the nucleus (blue) and F-actin (red), respectively. At least 1500 individual cells were imaged and analysed per condition in each experiment. Image analysis was performed using the InCell Morphology 1 analysis software (GE Healthcare). This software detects cells for morphology analysis by nuclear dye uptake, with quantification of cellular morphologies and fluorescent intensities determined from 1 or more intracellular stains (e.g., F-actin). Morphological and fluorescence intensity staining parameters were automatically recorded for every cell in the field, and these parameters were also automatically recorded numerically as average values per field and average values per well. Morphological and fluorescence intensity/distribution parameters that were recorded included 1/(form factor), cell area, cell gyration radius, cell/nuclear area, nuclear displacement,, IxA (nucleus and cytoplasm, N+C), intensity coefficient of variation (CV) and cell count. The definitions of these parameters are described in

Table 1. Background fluorescence was subtracted for fluorescence intensity measurements. In addition, a software-based filter was employed to exclude irregularly defined nuclei and unusually bright nuclear shapes.

2.4 Atomic force microscopy (AFM)

AFM experiments were performed using a NanoWizard II (JPK Instruments, Berlin, Germany) combined with a Nikon Eclipse Ti-E inverted microscope (Nikon Instruments, Surrey, UK). Force measurements were carried out on live A549 cells in a temperature-controlled liquid cell at 37ºC in contact mode. SiN cantilevers with a nominal spring constant of 0.06 N/m (DNP; Veeco Instruments, Santa Barbara, CA, USA) were used. On each cell, a 4x4 grid of force-distance curves was collected in at least 5 different positions [avoiding the nucleus and the very edge]. The maximum load was kept constant at 0.3 nN for all measurements and the range was maintained at 5 µm retraction after each indentation. The thickness of cells ranged from 5 µm to 10 µm and indentation did not exceed 10% of these values. Each force curve was fitted according to the Hertz model to obtain the Young's modulus at each point. For imaging cells were fixed using a mixture of 4% paraformaldehyde and 0.05% glutaraldehyde. Samples were imaged in PBS at room temperature using PPP-FM tips (NanoSensors, Neuchatel, Switzerland) with a nominal spring constant of 2.8 N/m. Samples were scanned in intermittent contact mode at a scan rate of 0.3 Hz at 512 × 512 pixels resolution. During imaging the AFM tip indents the cell membrane, producing deflection images in which the stiffer sub-membrane structures appear elevated, and in this way facilitates the acquisition of high resolution images, providing structural resolution on the nanoscale. Feedback gains were manually adjusted to obtain the best resolution in both height and deflection channels. Images

were processed and analysed using JPK Image Processing Software v3 (JPK Instruments). In the case of cell surface roughness measurements, at least fifteen 4×4 μm^2 areas of the topographical images were randomly selected for each condition and the root mean square (RMS) roughness (R_q) and peak-to-valley roughness (R_t) were calculated using JPK Image Processing Software v3. In order to minimise the impact of the slope of the areas, a high degree of flattening was employed.

2.5. Statistical analysis

Results are expressed as means ± S.D., compared using one-way analysis of variance (ANOVA) followed by the Student Newman–Keuls post-hoc test. $P < 0.05$ was considered as significant.

3. Results

3.1 Alveolar epithelial cells undergo EMT-associated morphological changes following exposure to TGF-β1 which are enhanced by collagen I

Using a HCA immunofluorescence imaging platform the morphological alterations induced following treatment with TGF-β1 were quantitatively evaluated. Analysis of cellular morphology was based on fluorescent staining of F-actin components of the cytoskeleton (Figure 1A-D). Of primary interest was the morphology parameter, 1/(form factor), which serves as a measure of cell roundness. Values range from 1 to infinity, whereby 1 reflects a perfect circle. A significant increase in 1/(form factor) was observed following stimulation of cells with TGF-β1 in comparison to those untreated (Figure 1E). This finding is in accordance with cells undergoing EMT and adopting a more spindle-shaped morphology. Moreover, culturing on collagen I served to significantly augment TGF-β1-induced increase in 1/(form factor) (Figure 1E). Additional morphological parameters were also evaluated, namely, cell area, cell gyration radius, ratio of cell/nucleus area, and nuclear displacement. Although cell area was not significantly altered (data not shown), the extent to which cells spread, as determined by cell gyration radius, was found to be significantly ($P<0.05$) enhanced following TGF-β1 exposure (Figure 1F). In line with increasing morphological alterations, stimulation of cells grown on collagen I was also shown to markedly enhance cell gyration radius in comparison to both untreated cells, and those exposed to TGF-β1 alone, in the absence of a collagen I matrix support (Figure 1F). In contrast, neither cell/nuclear area nor nuclear displacement was found to be influenced by TGF-β1 or collagen I (data not shown).

3.2 F-actin content and distribution is altered following TGF-β1 stimulation

Formation of F-actin stress fibres is a characteristic development in cells undergoing EMT. Hence, we also investigated the F-actin content and its distribution in cells upon stimulation with TGF-β1. The IxA (N+C) parameter effectively detects changes in cytoskeletal fluorescence intensity and correlates with alterations in F-actin content. Here, we observed an increase in fluorescence intensity of ~45% in those cells treated with TGF-β1 (Figure 2A). In addition to F-actin content, the distribution of F-actin was assessed. Two appropriate parameters were utilised to evaluate such changes; intensity spreading, which estimates the extent of fluorescence intensity near the boundary of the cell, and intensity CV, which describes the coefficient of variation of the fluorescence intensity of pixels within the cytoplasm (i.e., an even distribution of F-actin staining would give a low intensity CV, whereas formation of discrete F-actin structures would increase the value of this measurement). TGF-β1 stimulation evoked a significant increase in the F-actin content of cells, as illustrated by a higher IxA (N+C) value (Figure 2A). Although no significant change in intensity spreading was observed (data not shown), a marked increase in intensity CV was noted following treatment (Figure 2B). These findings were supported by visual inspection of immunofluorescence images, which revealed formation of discrete stress fibres within treated cells. Similarly, TGF-β1 exposure to cells grown on collagen I evoked increases in both IxA (N+C) value and intensity CV (Figure 2A and B). Interestingly, these effects showed apparent independence of growth support.

3.3 AFM identifies EMT-associated structural alterations in alveolar epithelial cells

Using AFM the sub-membranous components of the cytoarchitecture, in particular the stiffer filamentous structures were visualised. The AFM deflection images in Figure 3

show the morphology at the cell surface, indicating the sub-membrane structural organisation. In untreated samples, the cells are composed of poorly defined filamentous structures that appear as disordered ridges (Figure 3A and C). In contrast, TGF-β1 stimulated cells exhibit well-aligned filamentous structures directly beneath its membrane (Figure 3B and D). Given that actin is the predominant constituent of the cytoskeleton which localises under the cellular membrane, these observed structures are likely to be actin stress fibres.

Further insight into their topographical features was provided by three dimensional reconstructions of the corresponding height images. Cross-section analysis revealed distinct differences in surface height patterns between untreated cells and those stimulated with TGF-β1 (either on glass or collagen I). Untreated cells exhibited a relatively smooth curved surface, typical of an epithelial cell type (Figure 4A and C). In contrast, cells exposed to TGF-β1 showed a remarkably rougher surface profile interspersed with notable protrusions (Figure 4B and D) suggestive of EMT-related fibrous filamental structures running parallel to the cell's long axis.

An established quantitative method for demonstrating differences between surfaces is surface roughness. Using the JPK Image Processing Software v3 quantitative surface analysis was performed. Two parameters, root mean square (RMS) roughness (R_q), which represents the average of the measured height deviations taken within the evaluation length and measured from the mean line, and peak-to-valley roughness (R_t), a measurement of the absolute value between the highest and lowest peaks, were assessed. The data is summarised in Table 2. In support of analyses of image cross sections, these data demonstrate that TGF-β1-stimulation gave rise to significantly

(P<0.05) rougher cells (R_q=44.32 nm and R_t=203.43) compared to untreated cells (R_q=12.76 nm R_t=73.03). Moreover, this effect appeared to be significantly (P<0.05) augmented when cultured on a collagen I substrate (R_q=63.31 nm R_t=284.14).

3.4 TGF-β1 stimulation results in increased cell stiffness and is augmented by collagen I

Given the enhanced F-actin content at the surface of stimulated cells, it was anticipated that the local mechanical properties of these cells would change in response to these structural rearrangements. In contact mode, living cells were gently indented, and in doing so, a force was applied to induce cell membrane deformation. The level of deformation reflected the stiffness of the cell, and was illustrated in the resultant indentation force curves produced. Using JPK Image Processing software, Young's moduli were extracted from the force curves according to the classical Hertzian model. The results are summarised in Figure 5. Histograms of the apparent Young's modulus showed a log-normal distribution (Figure 5A-D). Stimulation of cells with TGF-β1 gave rise to a notable shift in population distribution towards higher Young's modulus values (Figure 5B and A). Prior to treatment, cells exhibited a stiffness of 8.3±1.1 kPa when cultured on glass. Similarly, those grown on a matrix of collagen I displayed a Young's modulus of 9.1±2.9 kPa. Following treatment, cell stiffness significantly increased, with a value of 21.5±5.2 kPa for those grown on glass. This represents more than a two-fold increase following TGF-β1 stimulation (Figure 5E). Interestingly, increases in cell stiffness were most apparent in cells treated with TGF-β1 and cultured on a collagen I substrate. Our data indicate that collagen I significantly (P<0.05) augments the pro-stiffening effects of TGF-β1 (Figure 5E). Together, these results confirm that actin filament organisation is a

determinant factor in the modulation of cell stiffness, and suggest that ECM interactions may also play a contributory role.

3.5 Increase in cell stiffness is strongly correlated with alterations in cell shape

Cell shape is thought to be an important determinant in cellular biomechanics. Using data obtained from both AFM and HCA analysis, we plotted values for 1/(form factor) against Young's modulus (Figure 6). A strong linear correlation between these two parameters was obtained (R^2=0.98). This correlative analysis indicates that the greater cells deviate from their cobblestone-like epithelial state towards a spindle-shaped mesenchymal phenotype, the more pronounced cell stiffness becomes.

4. Discussion

Alterations in the mechanical properties of tissues and living cells are associated with a number of pathological processes (Krouskop et al., 1998; Kilpatrick et al., 2002; Tajaddini et al., 2003; Samani et al., 2004). Fibrosis, characterised by a thickening and scarring of tissue, is a notable example. In the lung, an organ which exhibits unique mechanical properties crucial for breathing, fibrosis results in a marked increase in tissue stiffness [1]. The myofibroblast is the primary effector cell in IPF, and is responsible for synthesis, deposition and remodelling of ECM [2]. Although their exact origin remains unresolved, evidence continues to suggest that EMT may be a contributory source [11,19]. Here, in this study, application of AFM and HCA technologies has facilitated an entirely novel assessment of key mechano-cellular features of alveolar EMT, offering highly valuable insight into how the mechanical attributes of these transitioning cells are related to their underlying structure.

The cell cytoskeleton is a profoundly dynamic structure which is responsible for the determination of both cell shape and mechanical integrity [20]. Typically, every cell type has a specific size and shape, with each holding a specialised function. Under circumstances whereby cells are unable to maintain their inherent shape, such functions are compromised. In this way, modifications of cytoskeletal structure can potentially give rise to changes in cell behaviour and phenotype. In line with this, and in agreement with previous studies [19,21,22], our investigations revealed that TGF-β1 stimulation of alveolar epithelial cells induced dramatic changes in cytoskeleton

organisation. The importance of the cytoskeleton in governing cell shape was emphasised by our quantitative analysis of cellular morphology, which highlighted a striking deviation away from the cobblestone appearance associated with epithelial cells, to a more elongated fibroblast-like form, following TGF-β1 exposure. Moreover, stimulated cells were shown to exhibit an enhanced capacity to spread, suggestive of a greater migratory potential, and characteristic of the mesenchymal phenotype [23].

Immunofluorescence analysis of the cytoskeletal component, F-actin, revealed rearrangements in its organisation in accordance with transition to a (myo)fibroblast state. Before treatment, the majority of F-actin was localised to the periphery near intercellular junctions. TGF-β1 induced disruption of this arrangement, giving rise to increased numbers of F-actin stress fibres, assembled parallel to the long axis of cell bodies. Multiparametric analysis using a HCA platform permitted comprehensive quantitative assessment of these changes. Both F-actin intensity and distribution were shown to be significantly altered following TGF-β1 exposure. Additionally, culturing cells on collagen I appeared to enhance TGF-β1's EMT-inducing effect. Of note, use of the image-based HCA technology facilitated a rapid, accurate and quantitative evaluation of the EMT-related changes in cytoskeletal architecture. To our knowledge, this represents the first such wide-ranging assessment of a series of morphological and fluorescence intensity parameters in the context of alveolar EMT.

Recent studies suggest that cellular mechanical properties may serve as novel biological markers of cell phenotypes, reflecting changes in differentiation or cellular transformation [24,25]. In this regard, AFM has emerged as a powerful technique

capable of providing valuable insights into the nanomechanical properties of cells. Using AFM indentation we quantitatively assessed cellular elasticity in response to TGF-β1. Previously, it has been shown that spindle-shaped cells tend to be stiffer than round cells [26]. In agreement with this, we observed a significant increase in Young's modulus in those cells stimulated with TGF-β1. These findings corroborate the suggestion that EMT gives rise to stiffer cells, and supports recent observations in epithelium of the kidney [27]. Such changes in the mechanical properties brought about by the phenotypical transformation process may be attributed to the increase in the amount of organised actin filaments or stress fibres, which appear as stiff cables in a soft matrix. Indeed, a number of reports indicate that cytoskeletal structures, and in particular F-actin, are intimately involved in determination of cellular mechanics. Notably, Hertz's model was utilised to analyse data from the indentation of cells by AFM. Whilst assumptions of homogeneity, isotropicity, and material elasticity cannot be wholly satisfied, it nevertheless offers a good estimate of the Young's modulus [28]. In particular, it should be noted that at thinner cellular sections, any Young's modulus values acquired are under a significantly greater influence of the substrate which lies beneath [29]. This is particularly so at the most peripheral regions of the cell. In order to minimise such occurrences, measurements at the cell periphery were avoided. Moreover, it was ensured that the depth limit of indentation did not exceed 10% of the sample thickness [30], thus guaranteeing that the maximum load was carefully controlled.

Previous studies indicate that basement membrane architecture is critical in maintaining an epithelial phenotype, and that alterations in its composition may promote phenotypic change [10]. Collagen I is the most common component of the

ECM and its production is markedly up-regulated in fibrotic lungs. Our findings reveal that cultivation of alveolar epithelial cells on a collagen I substrate promote a significantly greater increase in cell stiffness in response to stimulation with TGF-β1, than when grown on glass. In addition to cell shape and motility, it is acknowledged that the mechanical properties of living cells may be influenced by biochemical and physical cues in their surroundings [31]. In this regard, the ECM appears to be an important determinant. Indeed, McPhee and colleagues [31] have recently shown that fibroblasts cultured on fibronectin show notably higher stiffness in comparison to those grown on glass. Our findings lend further support to an important role for the ECM in determining cell biomechanics. In addition, in agreement with previous findings [11-13] it appears that such cell-matrix interactions may facilitate TGF-β1-induced EMT. Although not yet established, contact to a collagen I matrix may serve to activate EMT-related signalling pathways, and in this way promote a greater observable effect upon TGF-β1 exposure.

In conclusion, our results illustrate that treatment of alveolar epithelial cells with TGF-β1 significantly augmented the Young's modulus of living cells. Moreover, our analysis reveals that the ECM component, collagen I, significantly amplifies the effects of TGF-β1. In light of the fact that cellular elasticity is strongly influenced by cell shape and cytoskeletal structure, we examined the morphology and organisation of these structures upon exposure to TGF-β1. Quantitative analysis revealed significant increases in F-actin content and distribution together with changes in cell shape. Importantly, use of both AFM and HCA permitted kinetic monitoring *in vitro* of live cells in real time and fixed cells, and in this way facilitated the measurement of novel and distinct events associated with EMT of alveolar epithelial cells. Moreover,

this complementary approach showed high precision, accuracy and reproducibility, allowing measurements to be made directly at the individual cell level, thus minimising artefact and ensuring they are reflective of cell effects. To our knowledge, it represents one of the first such studies of this kind in the context of alveolar EMT. Collectively, these analyses indicate that the mechanical dynamics of transitioning alveolar epithelial cells are greatly controlled by the cytoarchitecture, as evidenced by the strong correlation between cellular elasticity and cytoskeletal arrangement.

Acknowledgements

The authors would like to thank Dr. Maarten van Es (Nanoscale Function Group, Conway Institute of Biomolecular and Biomedical Research, University College Dublin) for his assistance in use of the AFM.

References

1. Thannickal VJ, Toews GB, White ES, Lynch JP 3rd, Martinez FJ. Mechanisms of pulmonary fibrosis. Annu Rev Med 2004; 55: 395-417.

2. Selman M, Pardo A. The epithelial/fibroblastic pathway in the pathogenesis of idiopathic pulmonary fibrosis. Am J Respir Cell Mol Biol 2003; 29: S93-97.

3. Willis BC, duBois RM, Borok Z. Epithelial origin of myofibroblasts during fibrosis in the lung. Proc Am Thorac Soc 2006; 3: 377–382.

4. Willis BC, Borok Z. TGF-beta-induced EMT: mechanisms and implications for fibrotic lung disease. Am J Physiol Lung Cell Mol Physiol 2007; 293: L525–L534.

5. Kalluri R, Weinberg RA. The basics of epithelial-mesenchymal transition. J Clin Invest 2009; 119: 1420-1428.

6. Radisky DC, Kenny PA, Bissell MJ. Fibrosis and cancer: do myofibroblasts come also from epithelial cells via EMT? J Cell Biochem 2007; 101: 830-839.

7. Stricker J, Falzone T, Gardel ML. Mechanics of the F-actin cytoskeleton. J Biomech 2010; 43: 9-14.

8. Daley WP, Peters SB, Larsen M. Extracellular matrix dynamics in development and regenerative medicine. J Cell Sci 2008; 121: 255-264.

9. Hay ED. Extracellular matrix alters epithelial differentiation. Curr Opin Cell Biol 1993; 5: 1029-1035.

10. Zeisberg M, Bonner G, Maeshima Y, Colorado P, Müller GA, Strutz F, et al. Renal fibrosis: collagen composition and assembly regulates epithelial-mesenchymal transdifferentiation. Am J Pathol 2001; 159: 1313-1321.

11. Kim KK, Kugler MC, Wolters PJ, Robillard L, Galvez MG, et al. Alveolar epithelial cell mesenchymal transition develops in vivo during pulmonary fibrosis and is regulated by the extracellular matrix. Proc Natl Acad Sci U S A 2006; 103: 13180–13185.

12. Shintani Y, Maeda M, Chaika N, Johnson KR, Wheelock MJ. Collagen I promotes epithelial-to-mesenchymal transition in lung cancer cells via transforming growth factor-beta signaling. Am J Respir Cell Mol Biol 2008; 38: 95-104.

13. DeMaio L, Buckley ST, Banfalvi A, Flodby P, Minoo P, et al. Extracellular matrix (ECM) modulates epithelial-mesenchymal transition (EMT) of alveolar epithelial cells (AEC) Am J Respir Crit Care Med 2010; 181: A1223.

14. Dudek SM and Garcia JG. Cytoskeletal regulation of pulmonary vascular permeability. J Appl Physiol 2001; 91: 1487–1500.

15. Krouskop TA, Wheeler TM, Kallel F, Garra BS, Hall T. Elastic moduli of breast and prostate tissues under compression. Ultrason Imaging 1998; 20: 260–274.

16. Kilpatrick, D, Xu C, Vito R, Glagov S. Correlation of mechanical behaviour and MMP-1 presence in human atherosclerotic plaque. J Mech Med Biol 2002; 2: 1–7.

17. Tajaddini A, Kilpatrick DL, Vince DG. A novel experimental method to estimate stress-strain behavior of intact coronary arteries using intravascular ultrasound (IVUS). J Biomech Eng 2003; 125: 120–123.

18. Samani A, PlewesD A method to measure the hyperelastic parameters of ex vivo breast tissue samples. Phys Med Biol 2004; 49: 4395–4405.

19. Willis BC, Liebler JM, Luby-Phelps K, Nicholson AG, Crandall ED, et al. Induction of epithelial-mesenchymal transition in alveolar epithelial cells by transforming growth factor-beta1: potential role in idiopathic pulmonary fibrosis. Am J Pathol 2005; 166: 1321–1332.

20. Mofrad MRK, Kamm RD. Cytoskeletal mechanics: models and measurements. New York: Cambridge University Press; 2006, p. 1-252.

21. Kasai H, Allen JT, Mason RM, Kamimura T, Zhang Z. TGF-beta1 induces human alveolar epithelial to mesenchymal cell transition (EMT). Respir Res 2005; 6: 56.

22. Buckley ST, Medina C, Ehrhardt C. Differential susceptibility to epithelial-mesenchymal transition (EMT) of alveolar, bronchial and intestinal epithelial cells in vitro and the effect of angiotensin II receptor inhibition. Cell Tissue Res 2010; 342: 39-51.

23. Crosby LM, Waters CM. Epithelial repair mechanisms in the lung. Am J Physiol Lung Cell Mol Physiol 2010; 298: L715-731.

24. Darling EM, Zauscher S, Block JA, Guilak F. A thin-layer model for viscoelastic, stress-relaxation testing of cells using atomic force microscopy: do cell properties reflect metastatic potential? Biophys J 2007; 92: 1784–1791.

25. Tilghman RW, Parsons JT. Focal adhesion kinase as a regulator of cell tension in the progression of cancer. Semin Cancer Biol 2008; 18: 45–52.

26. Kidoaki S, Matsuda T. Shape-engineered fibroblasts: cell elasticity and actin cytoskeletal features characterized by fluorescence and atomic force microscopy. J Biomed Mater Res A 2007; 81: 803-810.

27. Thoelking G, Reiss B, Wegener J, Oberleithner H, Pavenstaedt H, et al. Nanotopography follows force in TGF-beta1 stimulated epithelium. Nanotechnology 2010; 21: 265102.

28. Kuznetsova TG, Starodubtseva MN, Yegorenkov NI, Chizhik SA, Zhdanov RI. Atomic force microscopy probing of cell elasticity. Micron 2007; 38: 824–833.

29. Dimitriadis EK, Horkay F, Maresca J, Kachar B, Chadwick RS. Determination of elastic moduli of thin layers of soft material using the atomic force microscope. Biophys J 2002; 82: 2798-810.

30. Oliver WC, Pharr GM. An improved technique for determining hardness and elastic modulus using load and displacement sensing indentation experiments. J Mater Res 1992; 7: 1564-1583.

31. McPhee G, Dalby MJ, Riehle M, Yin H. Can common adhesion molecules and microtopography affect cellular elasticity? A combined atomic force microscopy and optical study. Med Biol Eng Comput 2010; In press.

Figure Legends

Figure 1. Morphological analysis of the cytoskeletal architecture of alveolar epithelial cells. A549 cells were grown in 96-well plates and treated with TGF-β1 (5 ng/ml) for 48 h. Cells were then fixed using paraformaldehyde. For visualisation of F-actin, cell were labelled using TRITC-phalloidin (*red*) and their nuclei counter-stained using Hoechst 33258 (*blue*). Imaging and analysis was performed using InCell 1000™ Analyzer Cellular Imaging and Analysis platform. (A-D) Immunofluorescence staining for F-actin. Untreated cells showed a cobblestone appearance characteristic of epithelia. Following treatment, A549 cells exhibited loss of cell-cell contacts, acquisition of a more fibroblast-like morphology and formation of F-actin stress fibres. (E,F) Quantitative morphological analysis. TGF-β1 stimulation resulted in significant increases in both 1/(form factor), a measure of cell roundness, and cell gyration radius, a measure of cell spreading, and these effects were significantly augmented by culturing on a collagen I substrate. In all cases, means±SD from 3 independent experiments. * $P<0.05$.

Figure 2. TGF-β1 exposure affects F-actin content and distribution. Using InCell 1000™ Analyzer Analysis software the cytoskeletal fluorescence intensity and distribution was evaluated using relevant parameters. (A) Treatment with TGF-β1 (5 ng/ml) resulted in an increase in F-actin content as determined by the IxA (N+C) parameter. (B) Significant alterations in F-actin distribution upon TGF-β1 exposure was confirmed by a marked increase in the intensity CV parameter. These effects were found to be independent of growth support. In all cases, means±SD from 3 independent experiments. * $P<0.05$ versus uncoated; # $P<0.05$ versus collagen I.

Figure 3. Deflection images of alveolar epithelial cells measured by atomic force microscopy. A549 cells were grown on chamber slides and treated with TGF-β1 (5 ng/ml) for 48 h. Cells were then fixed using a mixture of paraformaldehyde and glutaraldehyde. Images were acquired using a cantilever with 2.8 N/m spring constant in PBS buffer at room temperature. (A-D)Visualisation of the cell ultrastructure revealed numerous distinct filamentous structures (arrows) in those cells treated with TGF-β1 on glass (*B*) or on collagen I (*D*), representative of F-actin stress fibres. In contrast, untreated cells (*A, C*) exhibited indistinct filament arrangements. Images shown are representative data of 3 independent experiments. *Bars 10 μm*.

Figure 4. Height images of alveolar epithelial cells obtained by atomic force microscopy. A549 cells were grown on chamber slides and treated with TGF-β1 (5 ng/ml) for 48 h. Cells were then fixed using a mixture of paraformaldehyde and glutaraldehyde. Images were acquired using a cantilever with 2.8 N/m spring constant in PBS buffer at room temperature. Cross-section analysis of three dimensional height projections of cells illustrated marked modifications in surface height patterns following stimulation with TGF-β1 (either on glass or collagen I). (A,C) Untreated cells exhibited a relatively smooth curved surface, typical of an epithelial cell type. (B,D) In contrast, cells exposed to TGF-β1 showed a remarkably rougher surface profile interspersed with notable protrusions, indicative of actin stress fibres. Images shown are representative data of 3 independent experiments.

Figure 5. Mechanical alterations in alveolar epithelial cells following TGF-β1 stimulation measured by atomic force microscopy. A549 cells were grown on glass

coverslips (uncoated or collagen I-coated) and treated with TGF-β1 (5 ng/ml) for 48 h. The elastic modulus of cells was measured in contact mode using a DNP tip. On each cell, a 4x4 grid of force-distance curves was collected in at least 5 different positions [avoiding the nucleus and the very edge] (A-D) Histogram showing the overall distribution of elastic modulus. Under all conditions cells exhibited a log-normal distribution. Following TGF-β1 treatment [either on (B) glass or (D) collagen I], a notable population shift to higher Young's modulus values was observed compared to those untreated on (A) glass and (C) collagen I. (E) Bar graph illustrating the average cell stiffness representing > 750 single force–distance curves (means ± SD). On glass, TGF-β1 stimulation resulted in an increased stiffness of more than a two-fold compared to untreated cells. Exposure to TGF-β1 of cells cultured on collagen I enhanced stiffness four-fold and significantly augmented the effect of TGF-β1 alone.

Figure 6. Correlation between cell stiffness and shape. Values for 1/(form factor) were plotted against Young's modulus. Analysis revealed a strong correlation between both parameters (R^2=0.98). Young's modulus values represent measurements from > 750 single force-distance curves. 1/(form factor) values represent data from 15 fields of >30 wells from three independent experiments. All values are expressed as means±SD.

Table 1. Description of InCell Analyzer 1000™ morphological and fluorescence intensity parameters.

Parameter	*Description*
1/(form factor)	Measure of cell roundness
Cell area	Area of the identified cell body
Cell gyration radius	Measure of the spread of the cell. Defined as the square root of the mean squared distance between the cells pixels and its centre of gravity
Cell/nuclear area	Cell to nucleus area ratio
Nuclear displacement	Distance between the nucleus's centre of gravity and the cells' centre of gravity, divided by the gyration radius of the nucleus
IxA (N+C)	The amount of light emitted by the whole cell. It is equal to cytoplasm average intensity multiplied by cell area
Intensity CV	Coefficient of variation of the fluorescence intensity of pixels within the cytoplasm
Intensity spreading	Intensity-based descriptor allowing estimation of the extent of intensity concentration near the boundary of the object

Table 2. Summary of calculated RMS roughness (Rq) and peak-to-valley roughness (Rt) values.

Condition	*R_q (nm)*	*R_t (nm)*
Uncoated	12.76±1.76	73.03±9.04
Collagen I-coated	15.38±1.36	79.92±5.98
Uncoated + TGF-β1	44.32±4.91	203.43±18.08
Collagen I-coated + TGF-β1	63.31±6.55	284.14±32.91

Using JPK Image Processing Software v3, Rq and Rt values were obtained from topographical images of cells. In all cases, values are expressed as means±SD. At least 5 cross section measurements were acquired on between 3 and 5 cells per independent experiment (n=3)

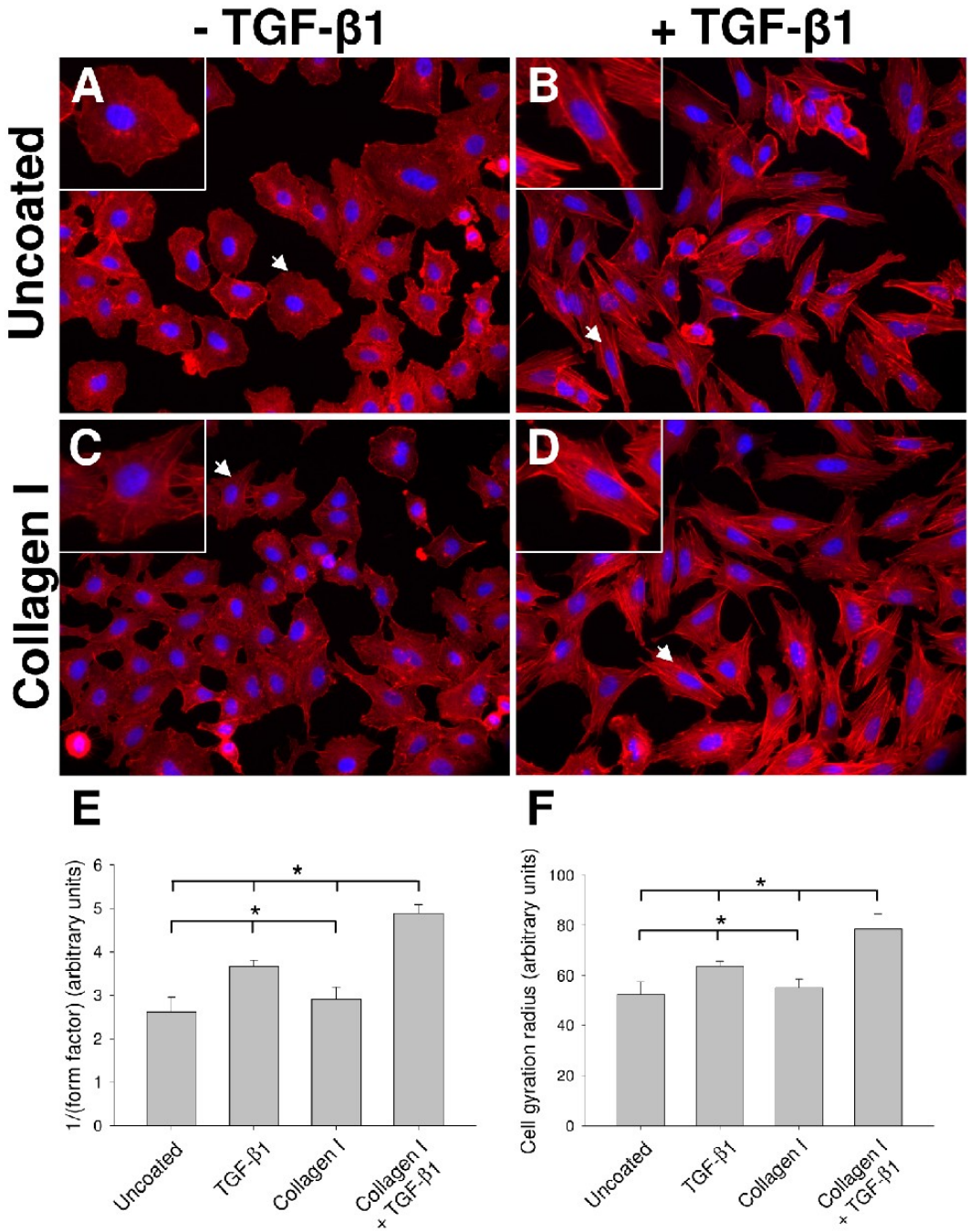
- TGF-β1
+ TGF-β1
Uncoated
Collagen I
A
B
C
D
E
F
1/(form factor) (arbitrary units)
Cell gyration radius (arbitrary units)
Uncoated
TGF-β1
Collagen I
Collagen I + TGF-β1
*

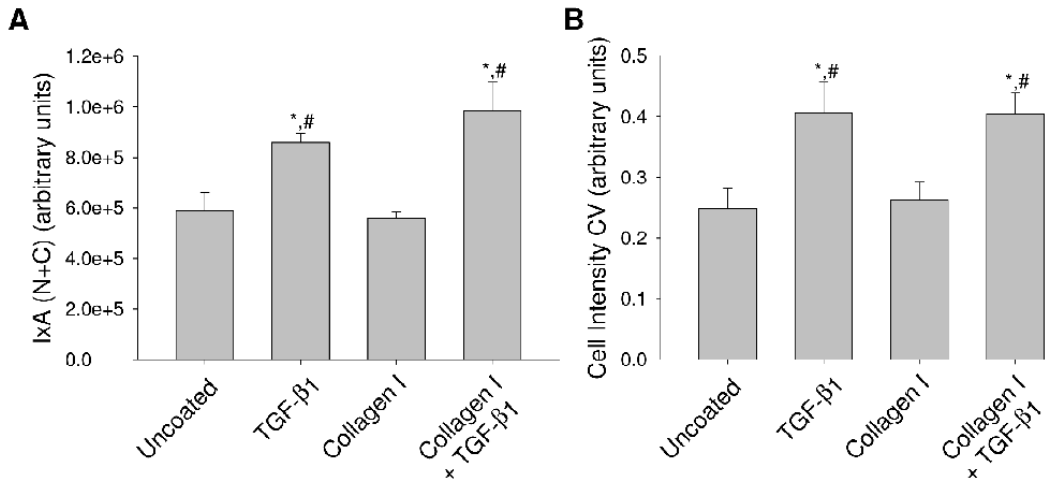

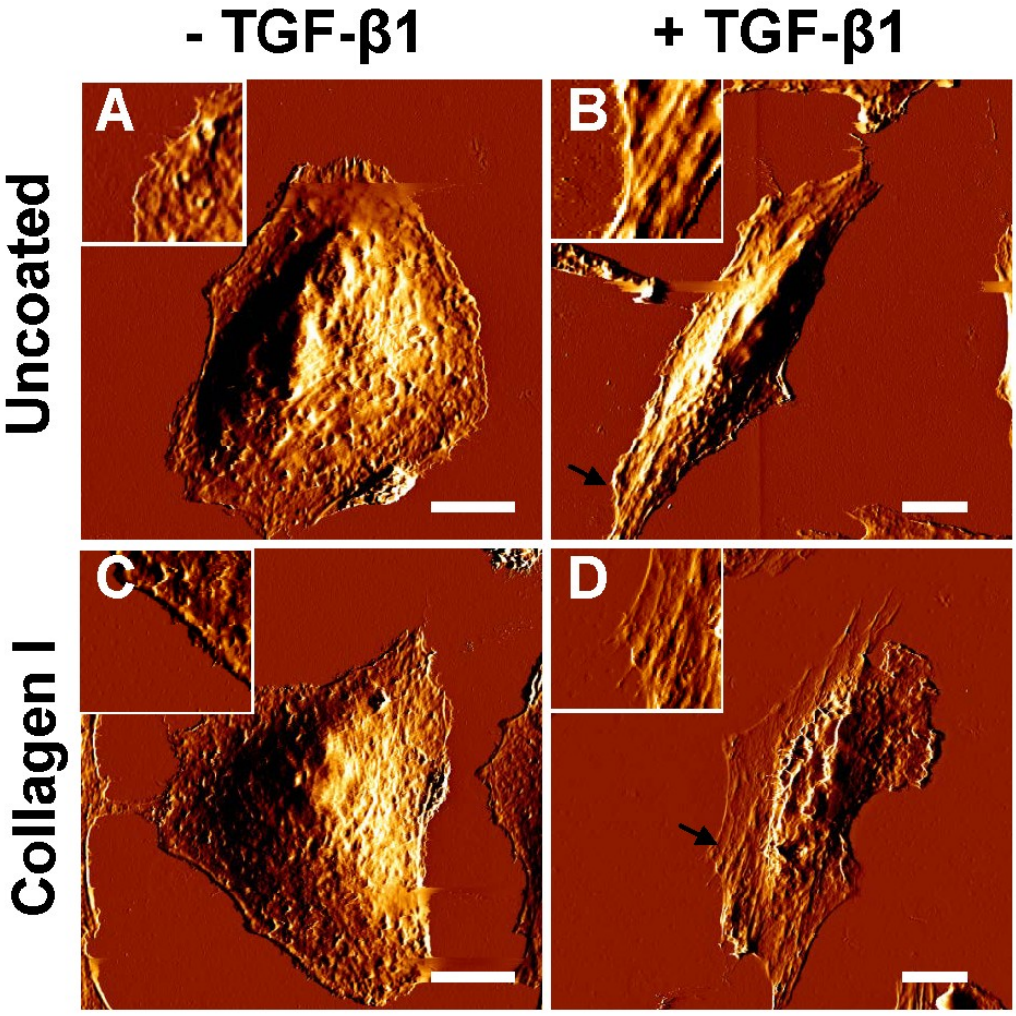

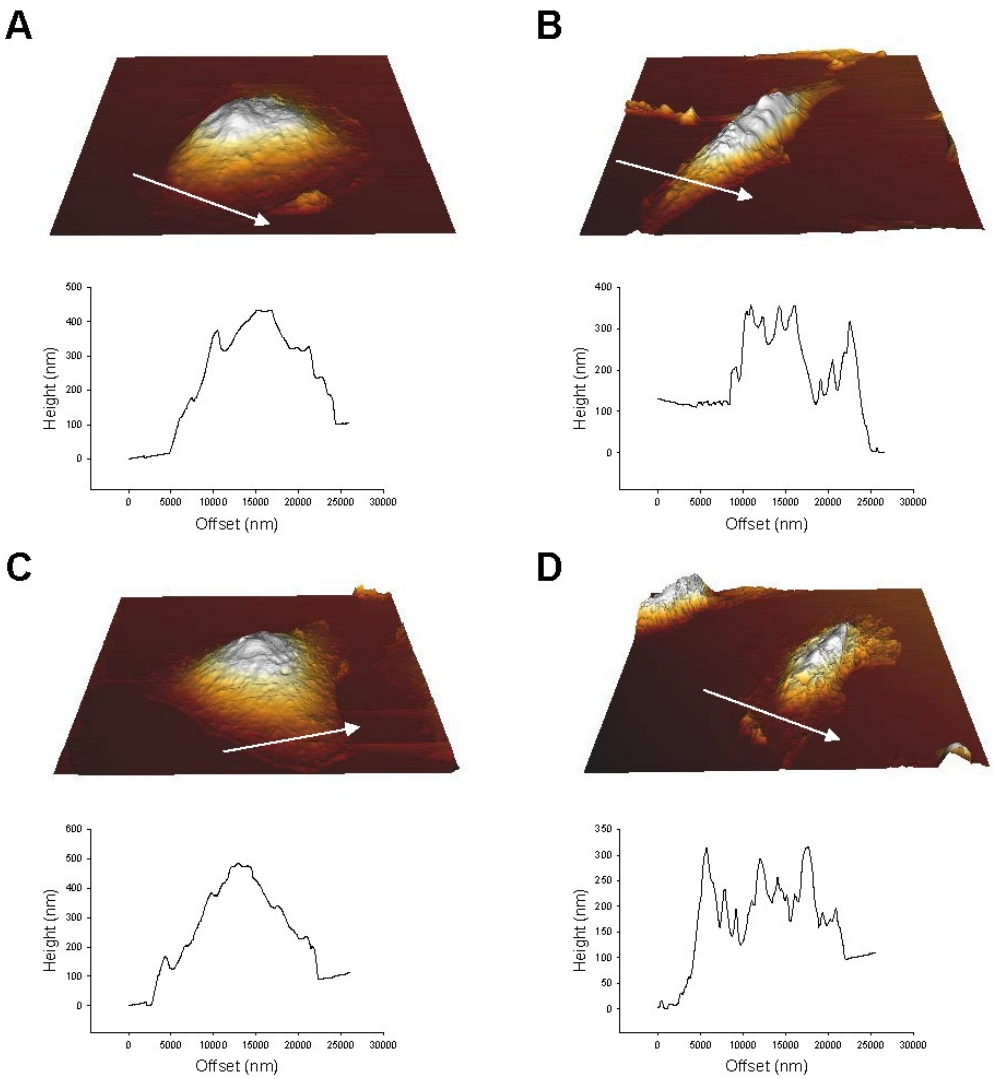

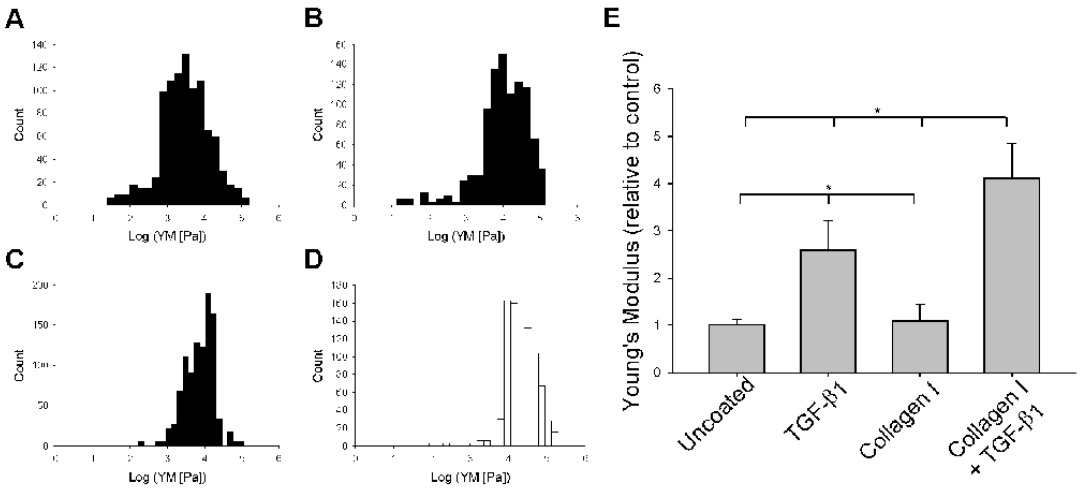

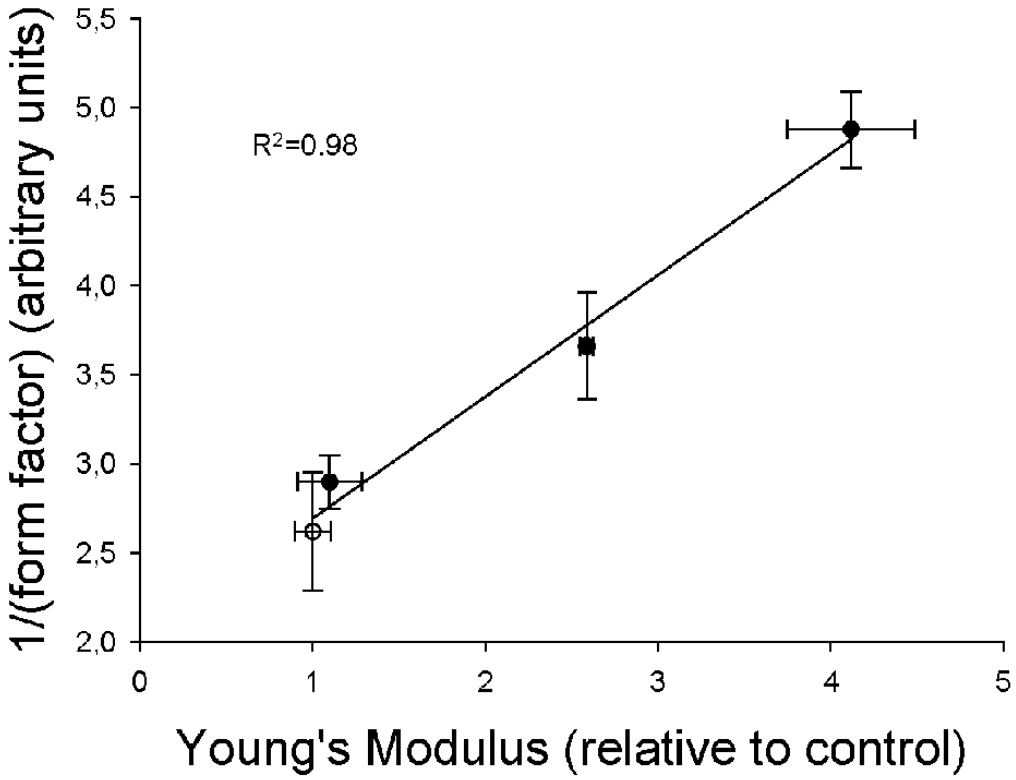

TGF-β1 exposure affects F-actin content and the cytoskeletal architecture of alveolar epithelial cells *in vitro*